

The effect of aluminum interlayer on weld strength, microstructure analysis, and welding parameters optimization in resistance spot welding of stainless steel 316L and Ti6Al4V titanium alloy

Iqbal Taufiqurrahman^{a*}, Turnad Lenggo Ginta^a, Azlan Ahmad^a, Mazli Mustapha^a, Ichwan Fatmahardi^a and Imtiaz Ahmed Shozib^a

^aDepartment of Mechanical Engineering, Universiti Teknologi PETRONAS, Perak, 32610, Malaysia

ARTICLE INFO

Article history:

Received 25 September 2021

Accepted 16 January 2022

Available online

16 January 2022

Keywords:

Resistance spot welding

Stainless steel

Titanium alloy

Mechanical properties

Microstructure

Welding parameters

Aluminum interlayer

Taguchi method

ABSTRACT

Stainless steel (SS) and Titanium alloy (Ti) are the most commonly used materials in many industrial fields such as the automotive and aerospace industry. Stainless steel has good corrosion resistance and titanium alloy has an extremely lightweight characteristic. The combination of both materials has become a tremendous innovation in the industrial sector. Resistance spot welding which has commonly applied in many industrial fields is a good consideration to join these two dissimilar materials due to the high efficiency that could be achieved by using this method. However, the way of joining these dissimilar materials should be carefully considered due to the significant difference in mechanical properties between SS and Ti. In the present study, 3 mm of SS316L and Ti6Al4V sheets were joint under the resistance spot welding method with an aluminum interlayer. The optimized welding parameters were provided under the Taguchi method L9 orthogonal array along with the mechanical properties' investigation. The optimum welding parameters were 11 kA of weld current, 30 Cycles of welding time, and 5 kN of electrode force which produced 8.83 kN tensile-shear load of the joint. The mechanical structure analysis shows the different morphology between stainless steel and titanium interfaces and the intermetallic compound layer was formed on the SS/Al and Al/Ti interfaces. The EDX analysis shows the atomic diffusion-reaction on the application of aluminum as an interlayer on the SS/Ti joint.

© 2022 Growing Science Ltd. All rights reserved.

1. Introduction

Nowadays, there has been a fast-growing concern in using alternative and hybrid materials in the automotive and aerospace industries. Current industries are looking for alternative materials that have the characteristics of lightweight material, good corrosion resistance, ease of fabrication, good weldability, etc. The properties of stainless steel 316L and Ti6Al4V titanium alloy based on the requirements as mentioned before are suitable for the automotive and aerospace industry applications. Considering the characteristics of stainless steel and titanium alloy, the product quality will significantly increase as well as the production cost efficiently achieved (Luz et al., 2020; Zhang et al., 2017). Therefore, combining these two materials is highly desirable for industrial applications. The most commonly used method in joining two pieces of metals is resistance spot welding (RSW). This method has been widely used in the automotive industry for joining frame and body works due to the semi-automated capability to increase the time efficiency. Besides the time efficiency that could be achieved by using the RSW method, the other benefit of using this method is that no additional weight on the joint is added compared with the

* Corresponding author. Tel.: +601128151637

E-mail addresses: iqbal_19001709@utp.edu.my (I. Taufiqurrahman)

riveting method which could give additional weight due to the rivet application itself (Han et al., 2010). However, since the resistance spot welding method is a thermal joining process that causes two base metals melted together to achieve the joining process, it becomes a tremendous challenge for researchers to join SS316L and Ti6Al4V. Different thermal and metallurgical properties of SS316L and Ti6Al4V produce poor weld quality and low joint strength. Mansor et al. (2018) has reported about the 0.5 mm thickness of SS316L and Ti6Al4V joints using the resistance spot welding method. The results showed that the maximum load of the joint was 378.25 N and produced interfacial failure mode (Mansor et al., 2018). Therefore, the direct joining process of stainless steel and titanium alloy should be avoided. However, this defiance could be avoided, and good joint quality could be achieved by inserting the interlayer in between the base metal's contact area.

The feasibility of applying interlayers such as Ni, Sn, Nb, Fe, and Al-based alloys in dissimilar resistance spot welding has been investigated by some researchers previously. The results showed that the application of interlayers brings significant improvement on the joint strength and increase weld quality (Houa et al., 2015; Oikawa et al., 1999; Qin et al., 2019; Sun et al., 2016). Aluminum alloy has good characteristics to be considered as an interlayer in industrial applications. The super lightweight, low cost, and ease of fabrication characteristics are suitable for industrial practical application. Successful application of aluminum interlayer to join dissimilar RSW of stainless steel SUS304 and pure titanium (Ti) has been done in a previous study and the result showed significant improvement compared with the joint without aluminum interlayer. Moreover, aluminum has a close atomic radius number with titanium and stainless steel which could produce diffusion-reaction and form an intermetallic compound layer between titanium and stainless steel (Tu et al., 2011). However, pure titanium is less suitable in the manufacturing industry compared with Ti6Al4V (Titanium Alloy Grade 5). Thus, the study about the application of aluminum alloy as an interlayer on dissimilar RSW of SS316L and Ti6Al4V is highly necessary and becomes a tremendous innovation.

During the experimental works, the design of the experiment is important to be considered. By using the resistance spot welding method, many parameter combinations could be applied to achieve the desired welding result. Thus, to reduce the experiment number and cost as well as increase efficiency, there are some designs of experiments could be adopted, such as the Taguchi method, Full Factorial, and Response Surface Methodology (RSM) (Mansor et al., 2018; Ravichandran et al., 2020; Shafee et al., 2015; Sharifi et al., 2020; Akbari et al., 2019; Kafshgar et al. 2021). In the present work, the joining of dissimilar materials using resistance spot welding becomes tremendous innovation. Although several researchers have investigated some of the dissimilar RSW processes, only a few studies have examined the joint between stainless steel and titanium alloy using interlayer. Moreover, the optimum welding parameters should be achieved during the resistance spot welding process to obtain the desired weld quality. The aim of this study is to investigate the effect of welding parameters on the physical and mechanical properties of dissimilar resistance spot welding of SS316L and Ti6Al4V titanium alloy using aluminum alloy interlayer. The present study uses the Taguchi method to analyze the optimum welding parameters due to experimental efficiency. By using three levels from three different factors, the Taguchi method could optimize the welding parameters using L9 Orthogonal Array which means only 9 runs of experiments. It will significantly reduce material cost and improve time efficiency compared with full factorial and RSM in which more than 20 experiments should be conducted. The optimized welding parameter is determined by the highest signal to noise (S/N) ratio which indicates the sensitivity of the optimum condition of the input factors in a controlled process (Mousavi Anijdan et al., 2018).

2. Materials and Methods

The 2 mm thick of aluminum alloy AA5754 was used as an interlayer in this present study to join the 3 mm thick of stainless steel 316L and 3 mm thick of Ti6Al4V titanium alloy using the resistance spot welding method. The welding experiment was based on the ASTM D1002 standard and under the lap joint configuration.

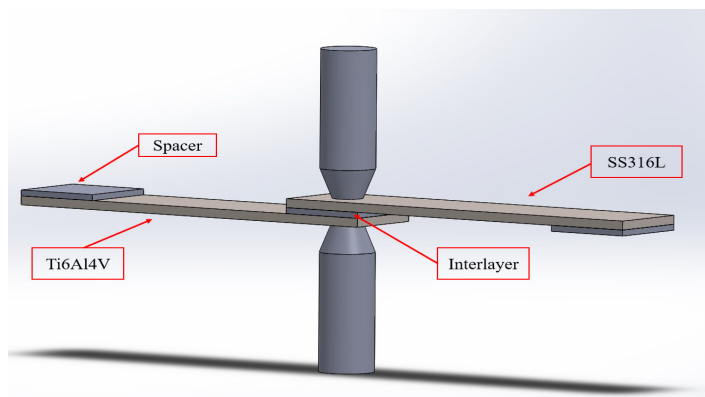


Fig. 1. Schematic configuration of SS-Ti resistance spot weld.

Fig. 1 shows the welding configuration of the present study. The joint between stainless steel and titanium alloy becomes challenging due to the different properties between both metals. Hence, the application of interlayers is necessarily important. The aluminum alloy AA5754 has a close atomic radius number with both titanium and stainless steel of 184, 187, and 194 pm, respectively. The bonding strength will significantly improve by applying the interlayer. After doing some trials and further research, the best thickness for the interlayer is 2 mm. Thus, 2 mm of AA5754 aluminum alloy was applied. In addition, the application of the spacers at the edge of the base metals are necessary during the tensile-shear test to make the grip and force applied become in line with the joint as shown in Fig. 1. The spacers were made from SS316L and Ti6Al4V with a thickness of 3 mm. Meanwhile, the chemical composition of each material is given in Table 1.

Table 1. Chemical composition of SS316L and Ti6Al4V titanium alloy

Element	SS316L	Ti6Al4V
Cr	17.68	-
Ni	12.6	-
Si	0.663	-
Mn	1.53	-
Mo	2.38	-
Co	0.121	-
Cu	0.211	-
W	0.029	-
P	0.02	-
S	0.003	-
Al	0.018	5.5-6.75
Ti	0.021	Balance
V	0.663	3.5-4.5
Fe	Balance	0-0.4
C	0.016	0-0.08
O	-	0.02
N	-	0.05

In the present study, DAIDEN Spot Welder SL-AJ 35-600 machine was used to perform resistance spot welding experiments. The experiments were conducted under the Taguchi L9 Orthogonal Array method which consists of 9 numbers of experiments. Three-level of welding parameters and one output response were considered in this method. The welding parameters are weld current, welding time, and electrode force, while the response is the tensile-shear strength of the joint. The numbers of welding parameters are 11-13 kA of weld current, 10-30 Cycle of welding time, and 3-5 kN of electrode force. Meanwhile, the squeeze and holding time were fixed at 40 and 30 cycles, respectively. The welding parameters used, and the experimental design of the Taguchi L9 Orthogonal Array is shown in Table 2 and Table 3, respectively. Furthermore, the analysis of variance (ANOVA) and regression analysis was investigated to provide the optimum welding parameters and the predictive result. Prior to the welding process, the samples were ground using SiC abrasive papers in order to remove surface contamination and obtain a smooth surface. Then, the samples were cleaned by using ethanol to remove the surface oxide layer and any other unnecessary contamination.

Table 2. Welding parameters of the experiments

Welding Parameters	Level 1	Level 2	Level 3
Weld Current (kA)	11	12	13
Welding Time (Cycles)	10	20	30
Electrode Force (kN)	3	4	5

Table 3. Experimental design of Taguchi L9 Orthogonal Array

Experiment Run	Weld Current	Welding Time	Electrode Force
1	11	10	3
2	11	20	4
3	11	30	5
4	12	10	4
5	12	20	5
6	12	30	3
7	13	10	5
8	13	20	3
9	13	30	4

The joint quality evaluation could be achieved by performing mechanical properties analysis. The first mechanical properties analysis was a tensile-shear test to obtain the tensile-shear strength of the joint. The test was applied using Zwick/Roell Universal Testing Machine with 50 kN of maximum load capacity and 10 mm/min of the ramp speed at room temperature. Each test was repeated three times under similar welding parameters to provide results accuracy. The next properties analysis was the microstructure and microhardness test. Prior to doing the microstructure analysis and microhardness test, the cross-section cuts were applied to the samples by using a wire cut machine for better results. Then, the cross-sectioned samples were prepared by grinding and polishing in sequence. The Carpenters etch was applied to the stainless-steel side and the Kellers etch was applied to the titanium and aluminum alloy side to obtain good microstructure images. The microstructure analysis was observed using a LEICA Metallurgical Microscope which covers the base metal, heat affected zone, and fusion zone area. Meanwhile, the micro-hardness test was conducted using a Vickers Micro-hardness machine with 200 gf of load and 15 seconds of dwell time. A total of 20 indentations were applied diagonally from stainless steel base metal to titanium alloy base metal.

3. Results and Discussion

3.1. SS-Ti joint strength analysis

The joint strength analysis between SS-Ti with aluminum interlayer under the resistance spot welding method has been done using a universal testing machine to measure the tensile-shear strength. The tensile-shear strength test is the most important step to identify the mechanical properties of the joint. By analyzing the peak load (N) of each experiment run, the effect of welding parameters could be observed. Other than that, the failure mode also could be identified by doing a tensile-shear test which describes the failure behavior of the joint. In this current study, the failure mode from all of the experiment run was identified as interfacial failure in which a crack propagates through the middle of the fusion zone and separates SS and Ti joint exactly at the faying surface (Huin et al., 2016). The failure mode and fracture surface of the SS-Ti joint with Al interlayer is shown in Fig. 2.

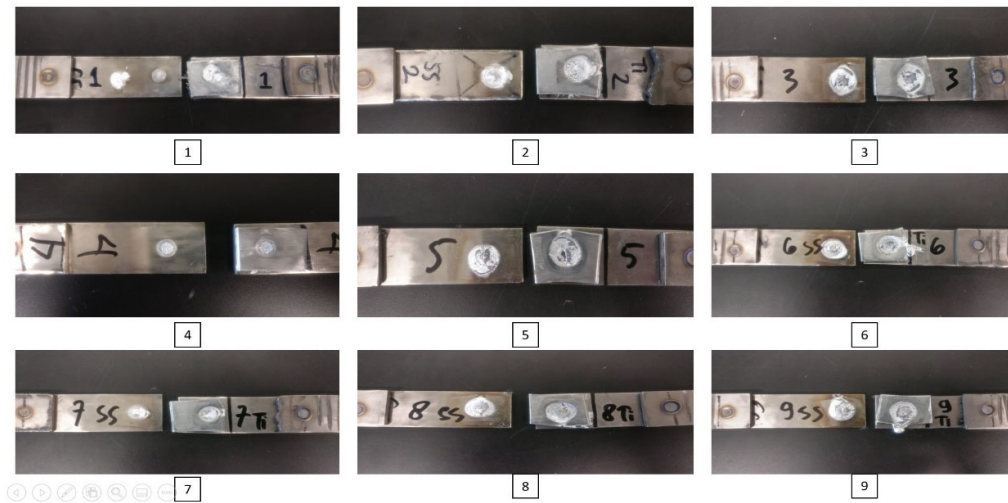


Fig. 2. Fracture surfaces appearance of the welded joints.

According to the failure mode examinations, the aluminum interlayer tends to adhere to the titanium alloy surface. The bonding between aluminum and titanium was better than aluminum and stainless steel. This happened due to the titanium alloy grade 5 consisting of aluminum alloy on its chemical composition. Moreover, due to the welding and heating process which causes aluminum alloy to melt, the diffusion-reaction between aluminum and titanium has occurred. Fig. 3 shows the appearance of the fracture surface on the SS-Ti joint. It shows that the aluminum interlayer remains to adhere to the titanium plate with only less amount of aluminum on the stainless-steel side.



Fig. 3. Faying surface appearance of the welded joint.

In this study, the effect of welding parameters brings a significant impact on the welded results in particular to weld diameter and tensile-shear strength. However, in resistance spot welding the requirement for weld diameter size should be $d > 4\sqrt{t}$, where t is the thickness of the plate. Fig. 4. shows the graph of the SS and Ti sides weld nugget diameter measurement. In general, the weld nugget diameter of the Ti/Al interface was larger than the SS/Al interface. This possibility happened due to both materials have different thermal properties which titanium allows more heat input than stainless steel one due to the SS316L has higher electrical resistivity than the Ti6Al4V (Mohanavel et al., 2020) (Khuenkaew & Kanlayasiri, 2019). A previous study revealed that the higher the welding current and longer welding time applied, the larger the weld nugget diameter formed (Sun et al., 2015). However, to produce more heat input, the electrode force should be reduced, thus the resistance gap between metal plates increases. Considering Fig.2, several samples which were welded under high heat input condition i.e. high weld current and long welding time (samples no. 5 to 9) experiencing severe expulsion on the aluminum interlayer. The expulsion could significantly decrease the joint strength. In this present study, the effect of the welding parameter combination also gives a significant impact on the weld joint strength. Fig. 5. shows the fluctuates graph of the SS-Ti welded joint peak load based on the design of the experiment runs. Since the characteristics of these two materials are different, to achieve the desired joint strength is quite challenging. The role of the design of the experiment will reveal the optimum welding parameters that could be used in the further applications. Based on the present work, the highest load was achieved on the experiment run number 3 which has 11 kA of weld current, 30 cycles of welding time, and 5 kN of electrode force which produces 8.71 kN load. However, this result proves that the application of the aluminum interlayer has successfully increased the tensile-shear load compared with the previous study which investigated SS316L and Ti6Al4V joint without interlayer and the maximum load was only 0.39 kN (Mansor et al., 2018). Thus, the joint strength of the SS316L and Ti6Al4V joint has 95.5% improvement according to the tensile-shear load.

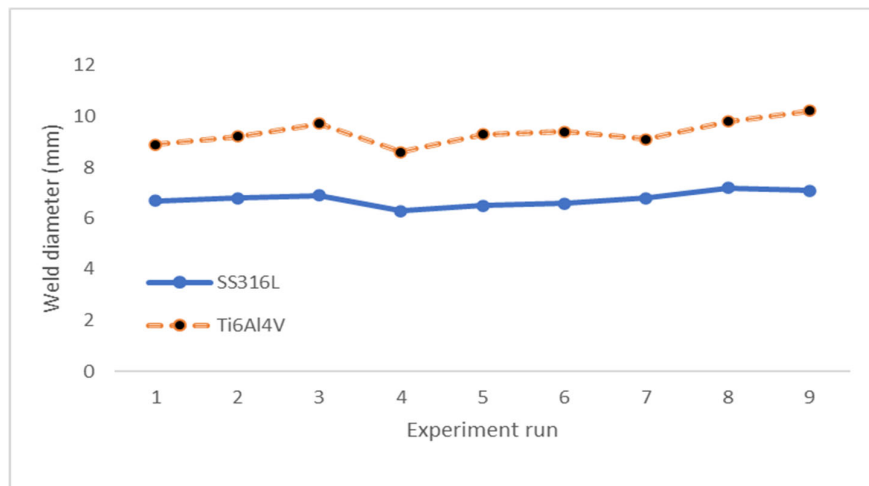


Fig. 4. Weld diameter measurements on SS and Ti sides.

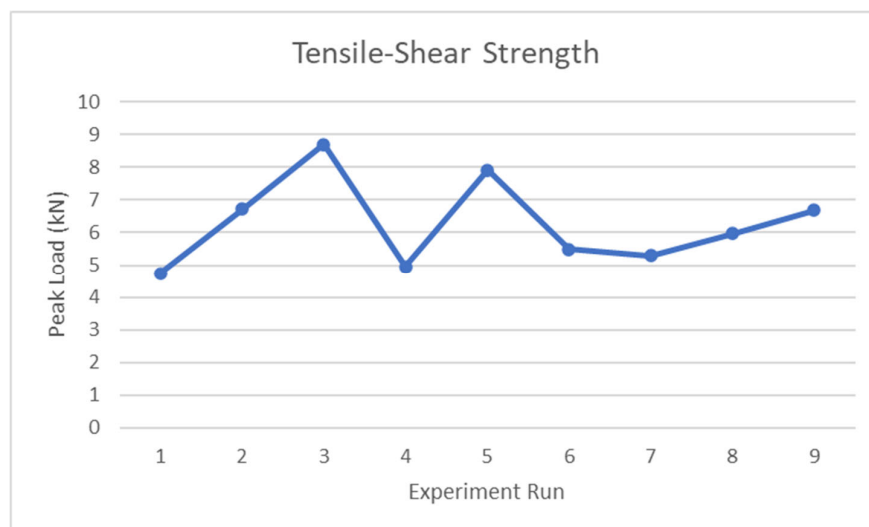


Fig. 5. The maximum load of the Taguchi method's based.

3.2. Welding parameters optimization

Since the welding parameters on the resistance spot welding method consist of many combinations, the optimization on this matter is necessary. Thus, the Taguchi method was used in this present study. L9 orthogonal array design of the experiments was used as shown in Table 3 previously. Basically, there are three types of loss functions in the Taguchi method that should be optimized: smaller-is-better, nominal-is-best, and larger-is-better. In this study, the larger-is-better function was used due to the aim of this optimization is to maximize the response by increasing the S/N (Signal to Noise) ratio. The objective of using the S/N ratio is to measure the effect of noise factors on the process parameters. The S/N ratio function is defined to calculate the deviation between the experimental value and the desired value. In this experiment, the larger-is-better function has an important role to define the optimum welding parameter combination (Neystani et al., 2019; Sahoo, 2014). The value of the response which is the peak load of the tensile-shear test results based on the Taguchi design of experiment and S/N ratio is shown in Table 4. The highest value of the S/N ratio indicates the highest peak load of the experiment results.

Table 4. Experimental results for tensile-shear strength and S/N ratio.

Experiment Run	Welding Parameters			Peak Load (kN)	S/N Ratio
	Weld Current	Welding Time	Electrode Force		
1	11	10	3	4.75	13.5339
2	11	20	4	6.73	16.5603
3	11	30	5	8.71	18.8004
4	12	10	4	4.95	13.8921
5	12	20	5	7.92	17.9745
6	12	30	3	5.49	14.7914
7	13	10	5	5.29	14.4691
8	13	20	3	5.98	15.5340
9	13	30	4	6.68	16.4955

Table 5 shows the response of signal to noise ratio. The highest value indicates the optimum level of the welding parameters. According to Table 5, welding time was the most influencing welding parameter which has the highest delta from the response of the S/N ratio. Based on the S/N ratio rank analysis, it shows that the most affecting parameters were welding time, electrode force, and weld current, respectively. Thus, from the response value in Table 5, the optimum welding parameters could be defined by selecting the highest value of the response of the S/N ratio. The optimum welding parameters in this study were 11 kA of weld current, 30 cycles of welding time, and 5 kN of electrode force.

Table 5. The response of signal to noise ratio (larger-is-better)

Level	Weld Current	Welding Time	Electrode Force
1	16.30	13.97	14.62
2	15.55	16.69	15.65
3	15.50	16.70	17.08
Delta	0.80	2.73	2.46
Rank	3	1	2

Table 6. ANOVA (Analysis of Variance) of the SS-Ti joint

Source	Degrees of Freedom	Sequential Sum of Squares	Adjusted Mean of Squares	F-value	P-value
Current	2	1.196	0.5982	1.02	0.496
Time	2	14.880	7.4402	12.63	0.073
Force	2	9.170	4.5849	7.78	0.114
Error	2	1.178	0.5890		
Total	8	26.425			
R-square	95.54%				

Meanwhile, Table 6 shows the analysis of variance (ANOVA) of the optimized welding parameters. The aim of the ANOVA is to investigate which of the welding parameters significantly affect the response of tensile-shear strength. The relative contribution of welding parameters in controlling the response of tensile-shear strength was provided in this analysis. Based on the ANOVA, the P-value revealed that welding time is the most dominant parameter since its value was 0.073, while

the significant parameter could be considered if the P-value is less than 0.05, whereas a P-value greater than 0.1 means that the parameter is insignificant (Pashazadeh et al., 2016). Compared with the weld current and electrode force P-value, welding time was the most significant parameter in this study. Moreover, the R-square is the coefficient of determination which could be used to measure the fitting degree of the regression equation. The value should be more than 0.8 and as close as possible to 1.0 in order to develop a linear model established by ANOVA is acceptable and the confidence interval value of the R-squared is not less than 95% (Jeang, 2015). From the analysis, Table 6 shows that the R-square was 95.54% which means the model developed was acceptable and the satisfactory of the model was achieved.

Fig. 6 shows the S/N ratio plot at each level of the control parameters. These plots show the correlation between each factor and the sum of S/N ratios. The highest point represents the optimum level of control parameters. In general, the highest S/N ratio indicates the best qualitative characteristic of tensile-shear strength. This plot is the representation of Table 5, which could be understood easily. Fig. 7 shows the normal probability plot vs. linear residual which shows that the residuals were located close to the straight line supporting the low number of errors which are still acceptable and implying that the model is significant and satisfactory achieved. From the normal probability plot, the linear regression analysis could be done by establishing the mathematical model for the predictive tensile-shear strength which could be beneficial for further application in industry to increase the time efficiency. The mathematical model was established using the multiple linear regression with the response was tensile-shear strength. The mathematical model is stated in Eq. (1).

$$\text{Peak Load} = 4.99 - 0.373 \text{ Current} + 0.0982 \text{ Time} + 0.950 \text{ Force} \quad (1)$$

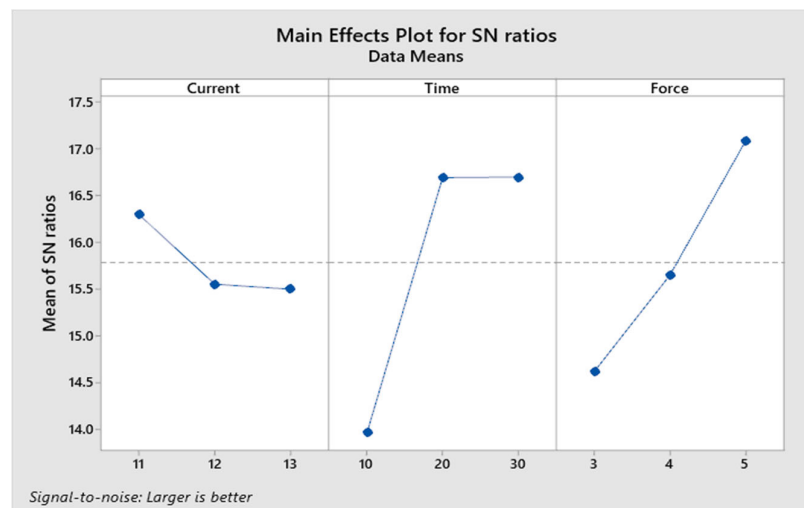


Fig. 6. Main effect plot for S/N ratios of SS-Ti joint.

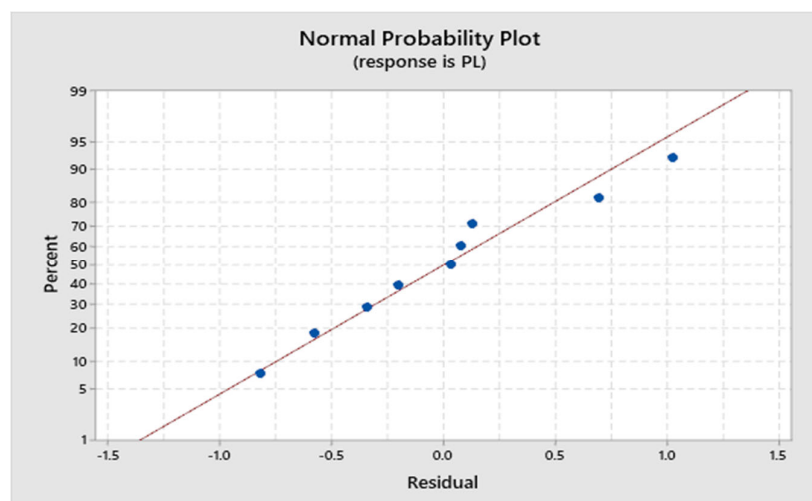


Fig. 7. Normal probability plot of the SS-Ti joint.

3.3. Confirmation test

The aim of doing parameter optimization is to obtain the optimum welding parameters on the resistance spot welding method. Therefore, the confirmation test is a mandatory step to be done after doing parameter optimization using the Taguchi method. The confirmation test was taken under the optimized welding parameters which are shown in Table 7. In addition, the comparison between the confirmation test and the predictive result was implemented to observe the difference between the predictive result and the actual result.

Table 7. The optimal welding parameter.

Weld (kA)	Current	Squeeze (Cycle)	Time (Cycle)	Welding (Cycle)	Time (Cycle)	Holding (Cycle)	Time (Cycle)	Electrode Force (kN)	Tensile-shear Load (kN)
11		40		30		30		5	8.83

The tensile-shear test of the confirmation test specimen using the optimum welding parameters shows that the peak load was 8.83 kN as shown in Fig. 8. Meanwhile, from the mathematical model calculation could be concluded that the maximum load for the predictive result is 8.58 kN. Thus, it was proven that the predictive result from the mathematical model was close with the actual result of the optimized welding parameters. It means that the mathematical model is valid and could be used for further application of the SS-Ti resistance spot welded joint.

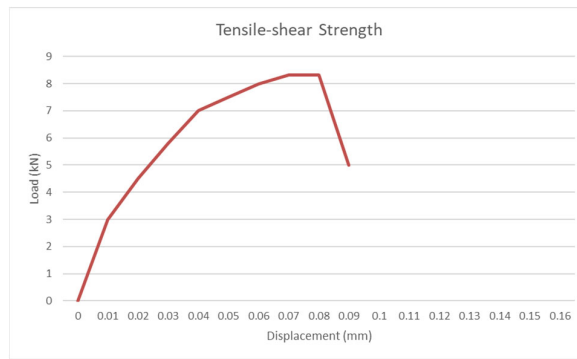


Fig. 8. The tensile-shear test result from the confirmation test specimen.

3.4. Microstructure observation

Microstructure analysis is very important in this present study to observe the phase transformation during the resistance spot welding process. The observed areas were base metal (BM), heat affected zone (HAZ), and the fusion zone (FZ) or nugget area. The interlayer microstructure was also included in this analysis. The schematic illustration of the microstructure analysis areas is shown in Fig. 9. The illustration consists of areas A (BM of SS316L and nugget), B (BM of Ti6Al4V and nugget), and C (interlayer area). The microstructure observation was carried out using LEICA Optical Microstructure under the cross-sectional cut of the welded joint. In this analysis, two welded samples were taken for further analysis. Experiment run no. 3 was taken with the consideration of the highest tensile-shear load, further called sample HL (High Load). Prior to the microstructure analysis, the Carpenters and Kellers etch were applied to the samples alongside with the proper grinding and polishing processes.

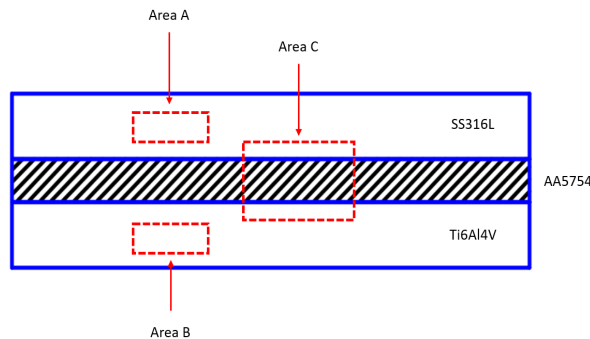


Fig. 9. Schematic illustration of the microstructure analysis area.

Fig. 10 is the illustrations of the cross-sectional cut of the sample HL. From the visual appearance of the sample, an unusual nugget formation has appeared. Both stainless steel and titanium alloy sides have their own weld nugget formation. This is due to the application of aluminium interlayer which caused both base metals to not be melted together due to the significantly different thermal properties between the base metals and the interlayer. Fig. 10A illustrates the nugget formation of the stainless-steel side. Meanwhile, Fig. 10B illustrates the nugget formation of the titanium alloy side. The sample HL showed that stainless steel has a smaller nugget area than that titanium alloy one. This is due to the contribution of the electrical resistivity in which stainless steel has higher electrical resistivity than titanium alloy, which means that the higher heat input was delivered to the titanium alloy, while the stainless steel has lower heat input. Moreover, the void has appeared on the sample HL which could be categorized as a weld defect. This condition was caused by the excessive heat input during the resistance spot welding process.

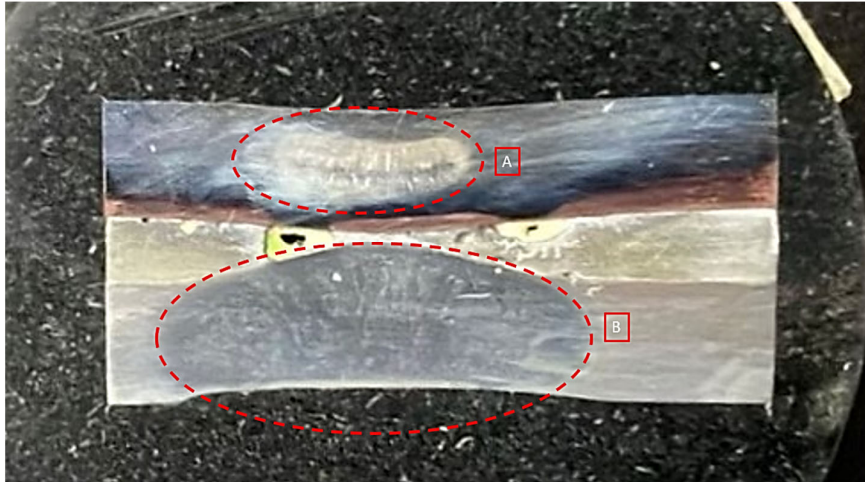


Fig. 10. The visual cross-sectional appearance of sample HL; (A) nugget formation of the stainless-steel, (B) nugget formation of the titanium alloy side.

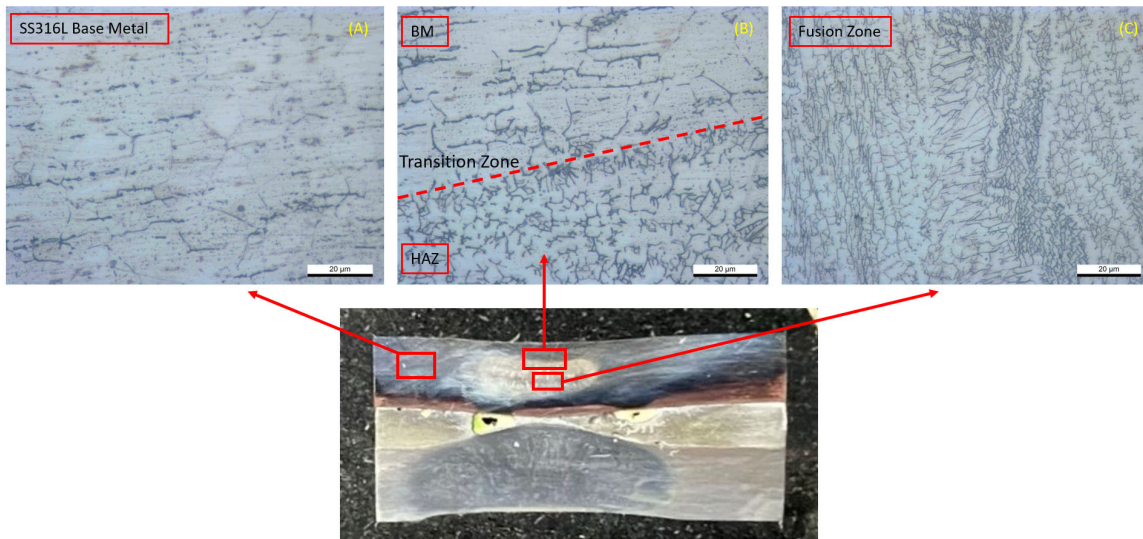


Fig. 11. Microstructure analysis of area A; (a) base metal; (b) transition zone; (c) fusion zone.

Moreover, in order to evaluate the effect of welding parameters on the morphology of the welded joint, further investigation was implemented by using an optical microscope on the specific areas. Fig. 11 illustrates the microstructure of the area A which is the SS316L area. The result indicated that SS316L experienced no phase transformation, owing to the compression-direction of the columnar grains and the formation of delta-ferrite (δ) instead. Fig. 11a depicts the microstructure phase consists of austenite (γ) dominantly which means there is no heat generated on the base metal area. Moving forward to the heat-affected zone (HAZ) area which is shown in Fig. 11b, the transition zone was clearly depicted under the 500x magnification of the optical microscope. It showed that the δ phase exhibits vermicular formation displacing the γ phase due to the heat input generated in this area. The fine δ vermicular phase was formed close to the edge of the BM-HAZ transition

zone, then it started to form a coarser δ phase right after passing through the transition line. The formation of the δ vermicular phase started to be dominant above the austenite phase. Moving further to the fusion zone of the SS316L area which is shown in Fig. 11c, the δ phase formation started to transform into the δ reticular morphology. However, the highest heat input generated was located in the fusion zone. Consequently, the formation of ferritic (δ) and sigma (σ) phases were dominant within the austenitic phase. The high heat input on the fusion zone constrained no phase transformation and the ferritic grain growth was exhibited instead. The ferritic grain growth produced coarser and narrow grains of the δ phase which is depicted in Fig. 11c. Similar phenomena were investigated in the previous studies using the stainless steel joint under the resistance spot welding method (Chen et al., 2017; Khuenkaew & Kanlayasiri, 2019). Meanwhile, the other portion of the reticular ferritic phase tends to become thinner and redissolves in the γ phase. The coarser ferritic grains of the stainless steel significantly weakened its strength due to the acicular grain growth formation (Charde & Rajkumar, 2013). Convincingly, the effect of heat input on the SS316L side of the SS316L-Ti6Al4V joint using aluminium interlayer has its own significant impact on the grain growth and phase transformation which leads to the different microstructure observation between the base metal, heat affected zone, and fusion zone.

On the other side, the microstructure of the Ti6Al4V side on area B of the schematic microstructure analysis was investigated in detail. Fig. 12 indicates the typical microstructure appearance based on the common three different areas; base metal, heat affected zone, and fusion zone. The difference between those three areas is generally easy to be identified, owing to the transition zone that appeared between the base metal and heat affected zone, moreover, the contrast has significantly appeared under the optical microstructure observation. Since the titanium alloy used is Ti6Al4V, thus it has a dual-phase of α phase and β phase or generally called $\alpha + \beta$ alloys. The presence of 6 wt% aluminium acts as an α phase stabilizer by increasing the $\alpha - \beta$ transformation temperature, meanwhile, the presence of 4 wt% vanadium acts as a β stabilizer. Therefore, the presence of aluminium and vanadium on the titanium alloy makes it more feasible and applicable to the industrial sector. Fig. 12a depicts the base metal area indicated by the dominant form of the α phase (indicated with the white colour of the grain boundaries), whereas a small percentage of β phase distribution was observed. This typical microstructure is similar to the annealed structure for the $\alpha + \beta$ titanium alloys. The morphology in the HAZ was a variety of primary α , primary β , and transformation of the β phase to some fine acicular α' phase. Fig. 12b indicates the transformation zone between the base metal and the heat-affected zone which is depicted with the red line on the image. The HAZ visually has a coarser morphology compared with that of the base metal, owing to the significant difference of the generated heat input. Fig. 12c indicates the microstructure of the fusion zone which has the coarsened grain structure due to the room-temperature cooling rate. The microstructure analysis showed that the higher percentage of the β phase was entirely transformed into a coarse acicular martensite α' phase which indicated the formation of the dominant straight line covering the primary α phase shown in Fig. 12c. The martensite α' phase formation leads to the increase of the titanium alloy hardness value.

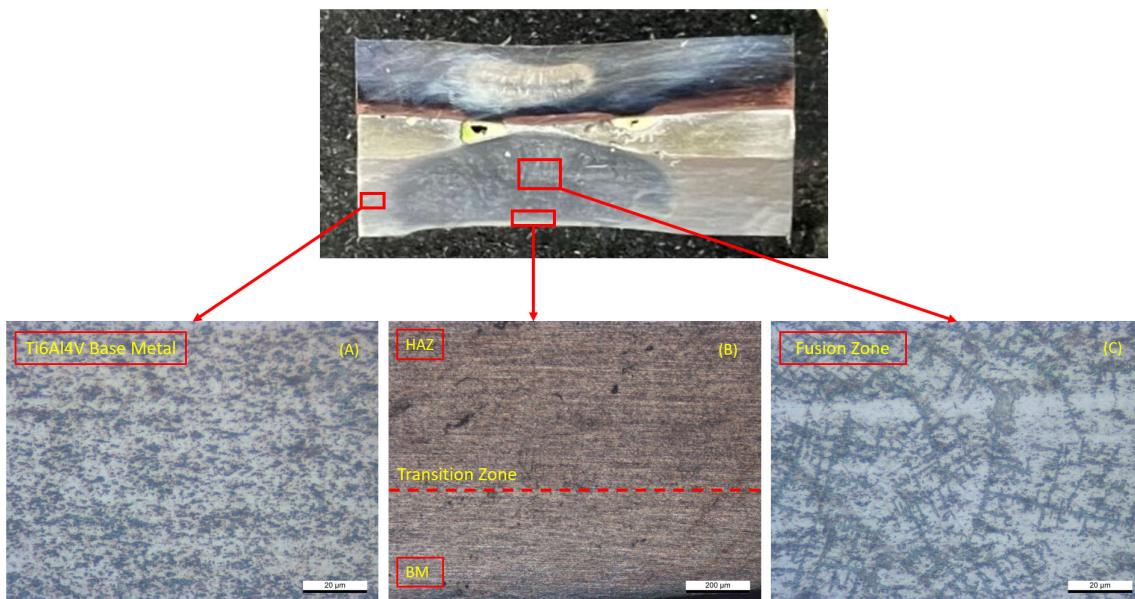


Fig. 12. Microstructure analysis of area B; (a) base metal; (b) transition zone; (c) fusion zone.

Fig. 13 shows the interface between the base metals and the interlayer. Fig. 13a indicates the formation of an intermetallic compound (IMC) layer on the SS/Al interface. A very thin IMC layer was formed as a part of aluminium interlayer reaction during the welding process. The intermetallic compound layer exhibited different morphology along the SS/Al interface. This IMC layer tends to create microstructural bonding between SS and Al which increases the joint strength. Similar morphology was also investigated by Zhang et al. using the high strength steel and aluminium joint (Zhang et al., 2011). However, the fairly thin IMC layer formation was varied along the welded area due to the unstable heat input generated and rapid cooling

on the fusion zone during resistance spot welding process. Fig. 13b shows the interlayer thickness and morphology on the SS/Ti welded joint. The microscope observation showed that the aluminium interlayer was squeezed tightly in between SS316L and Ti6Al4V. The aluminium interlayer thicknesses were also different along the welded area. Fig. 13b depicted the thinnest interlayer as 210.8 μm which is located in the middle of the welded zone owing to the highest heat input location and the highest electrode force distribution. Fig. 13c illustrates the morphology of the Al/Ti interface under the microscope observation. A clear border line was depicted between aluminium and titanium alloy interface. The diffusion-reaction has occurred during the welding process. The composition of aluminium diffused to the titanium and vice versa. Reticular morphology of titanium alloy formed on the aluminium interface, owing to the close atomic radius number between titanium and aluminium of 187 and 184, respectively. Besides, the composition of the titanium alloy also consists of aluminium as an α phase stabilizer. This phenomenon leads to the increase of the bonding between Al/Ti interfaces. Moreover, it was evident in Fig. 2 which showed that the aluminium interlayer has higher bonding strength to the titanium alloy side from all Taguchi based welding experiments. Therefore, it can be concluded that the application of aluminium interlayer brings significant improvement on the joint quality between SS316L and Ti6Al4V.

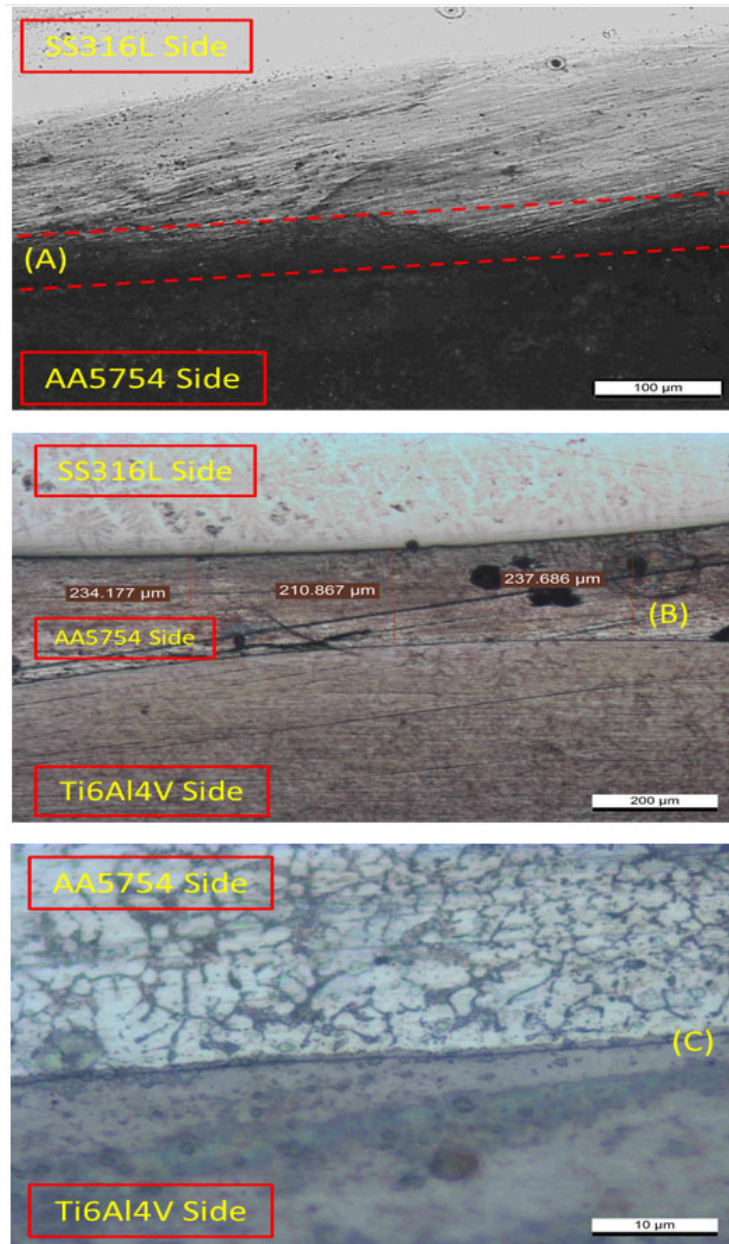


Fig. 13. Microstructure analysis of area C; (a) IMC layer of SS-Al side; (b) interlayer width; (c) Al-Ti diffused zone

3.5. Effect of Al interlayer upon the chemical composition of the SS-Ti joint

The chemical composition analysis has been done by the EDX observation at three different positions for both SS/Al and Al/Ti interfaces which started from the base metals of each SS316L and Ti6Al4V to the intermetallic compound (IMC) layer. The quantitative analysis of each interface is listed in Table 8 and Table 9 at the positions of spectrum 1, 2, and 3 shown in Fig. 14 and Fig. 15, respectively. Therefore, the chemical composition of the IMC layer between the base metal and the interlayer could be identified.

As shown in Fig. 14a, the EDX analysis has been done in three different positions starting from the base metal of SS316L, then moving forward to the SS316L base metal which closes to the intermetallic compound layer, and the third one was right on the SS/Al intermetallic compound layer. According to Table 8, spectrum 1 shows the dominant composition of 70.1 Wt% Fe and proved the composition of the SS316L base metal. In fact, the heat generated during the resistance spot welding process was not affecting the spectrum one position, thus there was no reactive diffusion occurred. Spectrum 2 indicated the composition of Fe was decreased from 70.1 to 40.6 Wt%. The heat generated started affecting the composition between stainless steel and aluminum alloy. On the other hand, spectrum 3 which is located specifically at the IMC layer of the SS/Al interface exhibited the diffusion of the Al composition. The 4.8 Wt% of aluminum has appeared on the intermetallic compound layer between stainless steel and aluminum alloy interface. Fig. 14b indicates the chemical composition on the IMC layer of the SS/Al interface. The exhibited aluminum on the IMC layer was controlled by the reactive diffusion between aluminum alloy and stainless steel. The reaction of both materials induced the formation of the Fe-Al intermetallic compound layer. Based on the Fe-Al binary phase diagram, the possible composition on this position could be Fe_2Al_5 and $FeAl_3$ which have the crystal structure of ordered BCC and BCC orthorhombic, respectively (Mehta, 2019; W. Zhang et al., 2011).

Table 8. EDX analysis results of the SS/Al intermetallic compound layer

Spectrum	Composition (Wt%)					
	Fe	Cr	Ni	O	C	Al
1	70.1	17.8	10.7	1.4	-	-
2	40.6	12.2	5.8	13.6	9.7	-
3	55.2	13.8	7.0	6.5	8.9	4.8

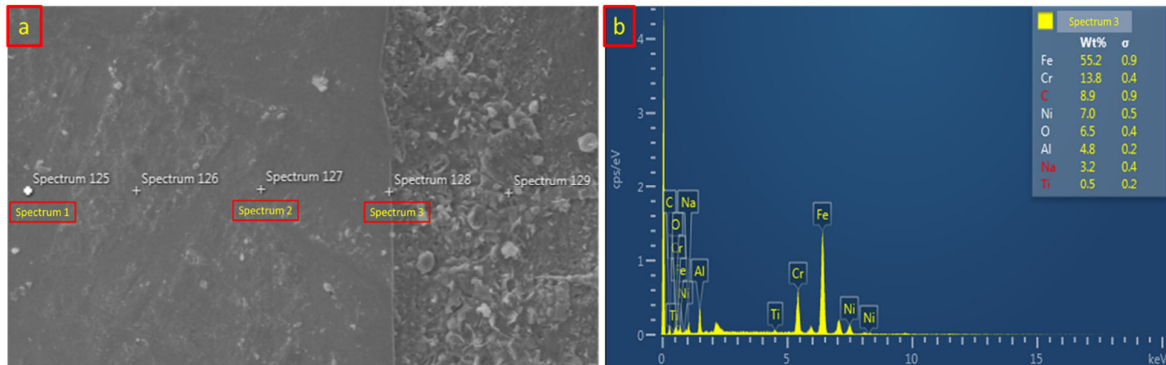
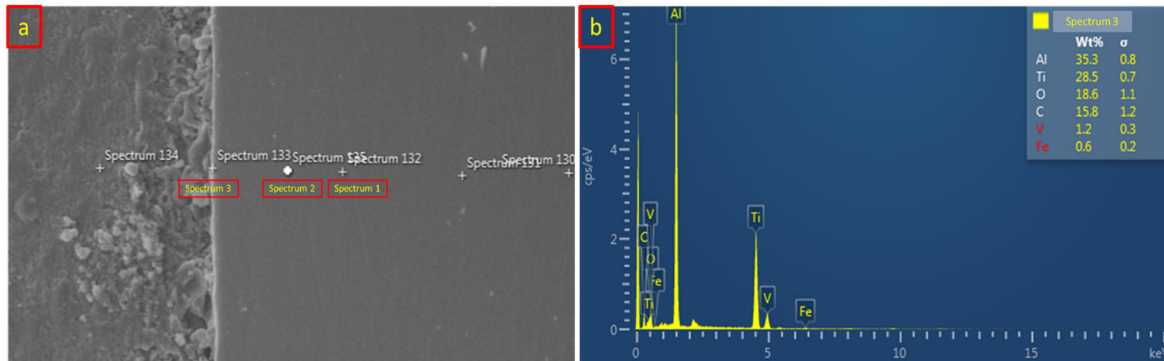


Fig. 14. (a) SS/Al EDX analysis distribution; (b) SS/Al EDX analysis result on the IMC layer.

Fig. 15a shows the SEM images and EDX analysis of the intermetallic compound layer on the Al/Ti interface. The specific position was similar to Fig. 14 which was divided into three different spectrum positions to compare the chemical composition of the base metal and the reaction on the IMC layer. According to Table 9, spectrum 1 indicated the high value of the Ti composition of 91.0 Wt% which means the position on spectrum 1 was dominated by titanium and followed by 5.4 Wt% aluminum and 3.6 Wt% vanadium. The composition of titanium decreases on the spectrum 2 due to the close location with the aluminum interlayer and the higher heat input generated. At spectrum 3 which is located exactly on the intermetallic compound layer, the composition of aluminum was increased significantly from 5.6 Wt% to 35.3 Wt%. Fig. 15b indicates the peak value of the aluminum refers to the XRD graph result. This analysis showed that the diffusion-reaction between aluminum and titanium has occurred due to several reasons. First, the close atomic radius leads the aluminum to diffuse easily to the titanium composition and vice versa to create stronger bonding on the Al/Ti interface. Second, the role of the aluminum as an α phase stabilizer forces aluminum to dissolve into the titanium composition due to the high heat input generated. The possible chemical composition on the IMC layer that could be identified is $TiAl_3$ due to the atomic diffusion-reaction which also has been investigated by the previous studies of the Ti/Al joint using the resistance spot welding process (Tu et al., 2011; Zhao et al., 2019).

Table 9. EDX analysis results of the Al/Ti intermetallic compound layer

Spectrum	Composition (Wt%)			
	Ti	Al	V	C
1	91.0	5.4	3.6	-
2	87.5	5.6	3.6	-
3	28.5	35.3	1.2	15.8

**Fig. 15.** (a) Al/Ti EDX analysis distribution; (b) Al/Ti EDX analysis result on the IMC layer.

4. Conclusion

The dissimilar resistance spot welding of 3 mm-thick austenitic stainless steel 316L and Ti6Al4V titanium alloy with 2 mm-thick aluminum alloy interlayer was successfully welded. The welding parameter has been optimized and the mechanical properties were investigated in detail. The conclusions of this study are summarized as follows:

1. Based on the Taguchi method and ANOVA, the optimized welding parameters are 11 kA of weld current, 30 cycles of welding time, 30 cycles of holding time, and 5 kN of electrode force which results in the tensile-shear strength of 8.83 kN from the confirmation test and 8.58 kN from the predictive result of the mathematical model.
2. The welded joint shows no fusion zone in the middle of the cross-sectional cut. Meanwhile, the fusion zone has appeared on both stainless steel and titanium alloy sides. The microstructure analysis shows three different zones of base metal, heat affected zone, and fusion zone. The phase was transformed from the dominant γ phase to the dominant δ phase on the stainless-steel side. Meanwhile, the higher percentage of the β phase was entirely transformed into a coarse acicular martensite α' phase on the titanium alloy side due to the excessive heat input. Moreover, the intermetallic compound layer was formed on both SS/Al and Al/Ti interfaces due to the heat input that caused the diffusion-reaction to occur.
3. The EDX analysis shows the chemical composition of the intermetallic compound layer on the SS/Al and Al/Ti interfaces. The results show that 4.8 Wt% of aluminum has appeared on the IMC layer of SS/Al which produces the possibility of the Fe_2Al_5 and FeAl_3 formation due to the reactive diffusion during the resistance spot welding process. Meanwhile, the composition of aluminum has significantly increased on the IMC layer of Al/Ti interface. 35.3 Wt% of aluminum and 28.5 Wt% of titanium were mixed on the Al/Ti IMC layer due to the atomic diffusion reaction between aluminum and titanium. These results proved that a good welding result has been successfully achieved by the application of aluminum as an interlayer on SS316L and the Ti6Al4V joint using the resistance spot welding method.

Acknowledgments

This work is fully supported by the funding given by Yayasan Universiti Teknologi PETRONAS (YUTP) no. 015LC0-052(YUTP).

References

- Akbari, M., Aliha, M. R. M., Keshavarz, S. M. E., & Bonyadi, A. (2019). Effect of tool parameters on mechanical properties, temperature, and force generation during FSW. *Proceedings of the Institution of Mechanical Engineers, Part L: Journal of Materials: Design and Applications*, 233(6), 1033-1043.
- Charde, N., & Rajkumar, R. (2013). INVESTIGATING SPOT WELD GROWTH ON 304 AUSTENITIC STAINLESS STEEL (2 mm) SHEETS. 8, 10.
- Chen, X., Li, J., Cheng, X., He, B., Wang, H., & Huang, Z. (2017). Microstructure and mechanical properties of the austenitic stainless steel 316L fabricated by gas metal arc additive manufacturing. *Materials Science and Engineering: A*, 703, 567–577.

- Han, L., Thornton, M., & Shergold, M. (2010). A comparison of the mechanical behaviour of self-piercing riveted and resistance spot welded aluminium sheets for the automotive industry. *Materials & Design*, 31(3), 1457–1467.
- Houa, L., Qiub, R., Cui, L., Shen, Z., & Li, Q. (2015). Microstructure and mechanical property of resistance spot welded joint between pure titanium and stainless steel with interlayer of Nb. *5th International Conference on Advanced Design and Manufacturing Engineering*, 6.
- Huin, T., Dancette, S., Fabrègue, D., & Dupuy, T. (2016). Investigation of the Failure of Advanced High Strength Steels Heterogeneous Spot Welds. *Metals*, 6(5), 111.
- Jeang, A. (2015). Robust product design and process planning in using process capability analysis. *Journal of Intelligent Manufacturing*, 26(3), 459–470.
- Kafshgar, A. R., Rostami, S., Aliha, M. R. M., & Berto, F. (2021). Optimization of Properties for 3D Printed PLA Material Using Taguchi, ANOVA and Multi-Objective Methodologies. *Procedia Structural Integrity*, 34, 71-77.
- Khuenkaew, & Kanlayasiri. (2019). Resistance Spot Welding of SUS316L Austenitic/SUS425 Ferritic Stainless Steels: Weldment Characteristics, Mechanical Properties, Phase Transformation and Solidification. *Metals*, 9(6), 710.
- Luz, F. S. da, Pinheiro, W. A., Monteiro, S. N., Candido, V. S., & Silva, A. C. R. da. (2020). Mechanical properties and microstructural characterization of a novel 316L austenitic stainless steel coating on A516 Grade 70 carbon steel weld. *Journal of Materials Research and Technology*, 9(1), 636–640.
- Mansor, M. S. M., Yusof, F., Ariga, T., & Miyashita, Y. (2018). Microstructure and mechanical properties of micro-resistance spot welding between stainless steel 316L and Ti-6Al-4V. *The International Journal of Advanced Manufacturing Technology*, 96(5–8), 2567–2581.
- Mehta, K. P. (2019). EARLY CAREER SCHOLARS IN MATERIALS SCIENCE 2019: REVIEW. *Jornal of Material Resources*, 34(1), 19.
- Mohanavel, V., Sundar, M., Pugazhendhi, L., & Ranganathan, K. (2020). Thermal and mechanical properties of titanium matrix composites synthesized through solid state technique. *Materials Today: Proceedings*, S2214785320340499.
- Mousavi Anijdan, S. H., Sabzi, M., Ghobeiti-Hasab, M., & Roshan-Ghiyas, A. (2018). Optimization of spot welding process parameters in dissimilar joint of dual phase steel DP600 and AISI 304 stainless steel to achieve the highest level of shear-tensile strength. *Materials Science and Engineering: A*, 726, 120–125.
- Neystani, R., Beidokhti, B., & Amelzadeh, M. (2019). Fabrication of dissimilar Fe-Cu-C powder metallurgy compact/steel joint using the optimized resistance spot welding. *Journal of Manufacturing Processes*, 43, 200–206.
- Oikawa, H., Ohmiya, S., Yoshimura, T., & Saitoh, T. (1999). Resistance spot welding of steel and aluminium sheet using insert metal sheet. *Science and Technology of Welding and Joining*, 4(2), 80–88.
- Pashazadeh, H., Gheisari, Y., & Hamed, M. (2016). Statistical modeling and optimization of resistance spot welding process parameters using neural networks and multi-objective genetic algorithm. *Journal of Intelligent Manufacturing*, 27(3), 549–559.
- Qin, Q., Zhao, H., Zhang, Y., Li, J., & Wang, Z. (2019). Microstructures and mechanical properties of Al-Mg₂Si-Si alloys resistance spot welded with Al-Si interlayers. *Journal of Materials Research and Technology*, 8(5), 4318–4332.
- Ravichandran, P., Anbu, C., Meenakshipriya, B., & Sathiyavathi, S. (2020). Process parameter optimization and performance comparison of AISI 430 and AISI 1018 in resistance spot welding process. *Materials Today: Proceedings*, S2214785320337585.
- Sahoo, A. (2014). Application of Taguchi and regression analysis on surface roughness in machining hardened AISI D2 steel. *International Journal of Industrial Engineering Computations*, 5(2), 295-304.
- Shafee, S., Naik, B. B., & Sammaiah, K. (2015). Resistance Spot Weld Quality Characteristics Improvement By Taguchi Method. *Materials Today: Proceedings*, 2(4–5), 2595–2604.
- Sharifi, E., Sadjadi, S. J., Aliha, M. R. M., & Moniri, A. (2020). Optimization of high-strength self-consolidating concrete mix design using an improved Taguchi optimization method. *Construction and Building Materials*, 236, 117547.
- Sun, M., Niknejad, S. T., Gao, H., Wu, L., & Zhou, Y. (2016). Mechanical properties of dissimilar resistance spot welds of aluminum to magnesium with Sn-coated steel interlayer. *Materials & Design*, 91, 331–339.
- Sun, M., Niknejad, S. T., Zhang, G., Lee, M. K., Wu, L., & Zhou, Y. (2015). Microstructure and mechanical properties of resistance spot welded AZ31/AA5754 using a nickel interlayer. *Materials & Design*, 87, 905–913.
- Tu, Y. M., Qiu, R. F., Shi, H. X., Zhang, X., & Zhang, K. K. (2011). Resistance Spot Welding between Titanium and Stainless Steel with an Aluminum Alloy Insert. *Advanced Materials Research*, 291–294, 964–967.
- Zhang, W., Sun, D., Han, L., Gao, W., & Qiu, X. (2011). Characterization of Intermetallic Compounds in Dissimilar Material Resistance Spot Welded Joint of High Strength Steel and Aluminum Alloy. *ISIJ International*, 51(11), 1870–1877.
- Zhang, X., Zhang, J., Chen, F., Yang, Z., & He, J. (2017). Characteristics of Resistance Spot Welded Ti6Al4V Titanium Alloy Sheets. *Metals*, 7(10), 424.
- Zhao, Y., Li, J., Qiu, R., & Shi, H. (2019). Growth Characterization of Intermetallic Compound at the Ti/Al Solid State Interface. *Materials*, 12(3), 472.

